ELectronics EXpress

A calibration method for frequency response mismatches in *M*-channel time-interleaved analog-to-digital converters

Husheng Liu[a)] **and Hui Xu**

College of Electronic Science and Engineering,

National University of Defense Technology, Changsha, 410073, China

a) *liuhusheng@nudt.edu.cn*

Abstract: Frequency response mismatches (FRMs) in time-interleaved analog-to-digital converters (TIADCs) generate undesired spurs degrading the performance of TIADCs. This paper introduces a digital calibration method for the FRM in *M*-channel TIADCs (*M*-TIADCs). This method exploits fixed differentiator finite-impulse response (FIR) filters and the Hadamard transform to reconstruct the mismatch induced error signal. The mismatch parameters are estimated utilizing a short training signal and the least square (LS) method. Our method is simpler in terms of implementation compared with conventional methods as cumbersome time-varying filters, complex signal processing and front-end hardware modifications are avoided. Numerical simulation results demonstrate the efficacy and efficiency of the proposed method.

Keywords: frequency response, time-interleaved ADC, mismatch, polynomial representation, Hadamard transform, least square

Classification: Circuits and modules for electronic instrumentation

References

[1] W. C. Black and D. A. Hodges: "Time interleaved converter arrays," IEEE J. Solid-State Circuits **15** (1980) 1022 (DOI: 10.1109/JSSC.1980.1051512).

[2] S. R. Velazquez, *et al.*: "A hybrid filter bank approach to analog-to-digital conversion," Proc. IEEE-SP Int. Symp. Time-Frequency Time-Scale Anl. (1994) 116 (DOI: 10.1109/TFSA.1994.467350).

[3] J. Matsuno, *et al.*: "All-digital background calibration technique for time-interleaved ADC using pseudo aliasing signal," IEEE Trans. Circuits Syst. I, Reg. Papers **60** (2013) 1113 (DOI: 10.1109/TCSI.2013.2249176).

[4] J. Li, *et al.*: "A digital timing mismatch calibration technique in time-interleaved ADCs," IEEE Trans. Circuits Syst. II, Exp. Briefs **61** (2014) 486 (DOI: 10.1109/TCSII.2014.2327333).

[5] C. Vogel and H. Johansson: "Time-interleaved analog-to-digital converters: status and future directions," ISCAS (2006) 3386 (DOI: 10.1109/ISCAS.2006.1693352).

© IEICE 2016

DOI: 10.1587/elex.13.20160668
Received July 5, 2016
Accepted July 25, 2016
Publicized August 8, 2016
Copyedited August 25, 2016

[6] K. Asami, *et al.*: "Technique to improve the performance of time-interleaved A-D converters with mismatches of non-linearity," IEICE Trans. Fundamentals **E92-A** (2009) 374 (DOI: 10.1587/transfun.E92.A.374).
[7] H. Johansson and P. Lowenborg: "A least-squares filter design technique for the compensation of frequency response mismatch errors in time-interleaved a/d converters," IEEE Trans. Circuits Syst. II, Exp. Briefs **55** (2008) 1154 (DOI: 10.1109/TCSII.2008.2002567).
[8] H. Johansson: "A polynomial-based time-varying filter structure for the compensation of frequency-response mismatch errors in time-interleaved ADCs," IEEE J. Sel. Topics Signal Process. **3** (2009) 384 (DOI: 10.1109/JSTSP.2009.2020554).
[9] K. M. Tsui and S. C. Chan: "A novel iterative structure for online calibration of M-channel time-interleaved ADCs," IEEE Trans. Instrum. Meas. **63** (2014) 312 (DOI: 10.1109/TIM.2013.2278574).
[10] S. Saleem and C. Vogel: "Adaptive blind background calibration of polynomial-represented frequency response mismatches in a two-channel time-interleaved ADC," Circuits Syst. I, Reg. Papers **58** (2011) 1300 (DOI: 10.1109/TCSI.2010.2094330).
[11] A. Bonnetat, *et al.*: "An adaptive all-digital blind compensation of dual-tiadc frequency-response mismatch based on complex signal correlations," IEEE Trans. Circuits Syst. II, Exp. Briefs **62** (2015) 821 (DOI: 10.1109/TCSII.2015.2435611).
[12] S. Singh, *et al.*: "Analysis, blind identification, and correction of frequency response mismatch in two-channel time-interleaved adcs," IEEE Trans. Microw. Theory Techn. **63** (2015) 1721 (DOI: 10.1109/TMTT.2015.2409852).
[13] S. Singh, *et al.*: "Frequency response mismatches in 4-channel time-interleaved ADCs: Analysis, blind identification, and correction," IEEE Trans. Circuits Syst. I, Reg. Papers **62** (2015) 2268 (DOI: 10.1109/TCSI.2015.2459554).
[14] A. Bonnetat, *et al.*: "Correlation-based frequency-response mismatch compensation of quad-TIADC using real samples," IEEE Trans. Circuits Syst. II, Exp. Briefs **62** (2015) 746 (DOI: 10.1109/TCSII.2015.2433472).
[15] C. Vogel and S. Mendel: "A flexible and scalable structure to compensate frequency response mismatches in time-interleaved ADCs," IEEE Trans. Circuits Syst. I, Reg. Papers **56** (2009) 2463 (DOI: 10.1109/TCSI.2009.2015595).

1 Introduction

Time-interleaved analog-to-digital converter (TIADC) [1] and hybrid filter bank analog-to-digital converter (HBF ADC) [2] are two similar schemes to achieve high sampling rate by employing several analog-to-digital converters (ADCs) operating in parallel. The TIADC scheme stands out because of its simplicity in hardware implementation. Ideally, the sampling rate of M-channel TIADC (M-TIADC) is M times of the sampling rate of a sub-ADC and without any performance loss. However, discrepancies between sub-ADCs referred to as mismatches arise because of the non-ideal manufactural process. These mismatches generate unwanted spurs distorting the input signal and degrading the performance of TIADC.

The TIADC architecture has been widely studied during the last three decades and a large number of methods are proposed to deal with the mismatch problem. The frequency independent mismatches, i.e. offset, gain and timing skew mis-

© IEICE 2016
DOI: 10.1587/elex.13.20160668
Received July 5, 2016
Accepted July 25, 2016
Publicized August 8, 2016
Copyedited August 25, 2016

matches, are dealt with in many papers e.g [3, 4] and references therein. Frequency response mismatch (FRM) is identified by Vogel and Johansson [5] as the main concern in future identification and calibration methods.

A frequency domain method is employed in [6] to deal with the mismatch problem in M-TIADC. The main drawback of this method is the lack of a configuration using a digital filter that is suitable for practical use. A least square (LS) filter design technique for FRM in M-TIADC is proposed in [7]. This method exploits the measured channel frequency responses to design a time-varying compensation filter based on the LS criterion. In [8], a polynomial-based time-varying structure is proposed for FRM compensation in M-TIADCs. This method avoids expensive on-line filter design by representing the frequency responses as polynomial series in $j\omega$. However, this method presumes the mismatch parameters are known thus no mismatches estimation method is presented. Moreover, a time-varying calibration filter is adopted in this method which means the variable multipliers must be updated at every sample.

The on-line method proposed in [9] calibrates the FRM in M-TIADCs by reserving some of the samples for reference signal. The main drawback of it is that the front-end hardware needs to be modified. In [10], a blind digital compensation method based on oversampling is proposed. However, it only works well for 2-TIADCs. Complex signal processing is employed in methods proposed in [11, 12, 13, 14] to estimate the mismatch coefficients and suppress spurious components.

This paper proposes a training signal based calibration method for FRMs in M-TIADCs. Our approach exploits fixed differentiator finite-impulse response (FIR) filters and the Hadamard transform to reconstruct the mismatch induced error signal and then subtract the error from the TIADC output. The mismatch coefficients are estimated by the LS method utilizing a short training signal which is a part of usual communication signals. Compared with existing calibration methods for M-TIADC, e.g. [8], our method has the following superiorities. Firstly, all signal processing units contained in our calibration structure are real and time-invariant, thus cumbersome complex and time-varying signal processing is avoided. Secondly, the mismatch parameters can be estimated on-line utilizing the training sequences contained in many communication signals, e.g. orthogonal frequency division multiplexing (OFDM) signals.

2 Model of M-channel TIADC

Fig. 1 shows the block diagram of an M-TIADC and the timing diagram of the sampling clocks. The analog input signal $x(t)$ (bandlimited to the Nyquist frequency) is sampled by M sub-ADCs operating in parallel with the same sampling period MT_s but the difference of T_s in sampling instants between adjacent channels. The sampled outputs of each sub-ADC are multiplexed to form $y[n]$ which is equivalently sampled with sampling period T_s. The quantization effect is neglected throughout the analysis in this paper. Ideally, $y[n]$ is the same as the uniformly sampled input signal $x[n] = x(nT_s)$. However, spur components stemming from the discrepancies between channel frequency responses $H_n(j\Omega)$ distort the signal and degrade the dynamic performance.

© IEICE 2016
DOI: 10.1587/elex.13.20160668
Received July 5, 2016
Accepted July 25, 2016
Publicized August 8, 2016
Copyedited August 25, 2016

IEICE Electronics Express, Vol.13, No.16, 1–12

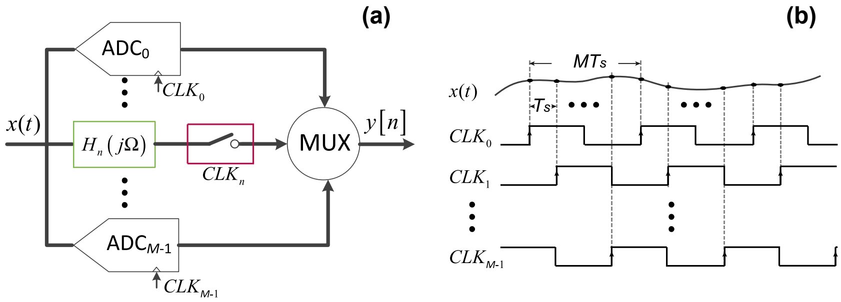

Fig. 1. (a) A time-interleaved ADC consists of M sub-ADCs. (b) Timing diagram of the sampling clocks.

The output $y[n]$ in the frequency domain is written as [15]

$$Y(e^{j\omega}) = \sum_{k=0}^{M-1} \breve{H}_k(e^{j(\omega - k\frac{2\pi}{M})})X(e^{j(\omega - k\frac{2\pi}{M})}) \tag{1}$$

with

$$\breve{H}_k(e^{j\omega}) = \frac{1}{M}\sum_{n=0}^{M-1} H_n(e^{j\omega})e^{-jkn\frac{2\pi}{M}} \tag{2}$$

and

$$H_n(e^{j\omega}) = H_n\left(j\frac{\omega}{T}\right), \quad -\pi \leq \omega < \pi, \tag{3}$$

where $X(e^{j\omega})$ is the discrete-time Fourier transform of $x[n]$.

2.1 Polynomial representation of frequency responses

In this paper, the frequency responses $H_n(e^{j\omega})$ are represented by the polynomial series in $j\omega$ as in [8], i.e

$$H_n(e^{j\omega}) = \sum_{p=0}^{P-1} \alpha_{n,p} D_p(e^{j\omega}), \tag{4}$$

where real-valued parameter $\alpha_{n,p}$ is the p-th coefficient of the polynomial series for channel n and $D_p(e^{j\omega}) = (j\omega)^p$, $(-\pi < \omega \leq \pi)$ is the p-th order discrete-time differentiator.

Fig. 2 shows a model of M-TIADC exploiting the polynomial representation of channel frequency responses. In this model, the frequency response mismatched M-TIADC with input signal $X(j\omega)$ is interpreted as P gain mismatched M-TIADC with differentiated input $X(j\omega)D_p(e^{j\omega})$, $p = 0, 1, \cdots, P-1$ and gain factors $\alpha_{n,p}$, and the output $y[n]$ is the sum of all the gain mismatched M-TIADC output. A calibration technique using pseudo aliasing signal is proposed in [3] for the gain and timing skew mismatches problem in M-TIADC. As the M-TIADC with FRMs is interpreted as P M-TIADC with gain mismatches, we can extend the method in [3] to deal with the FRMs problem.

2.2 Frequency response mismatches induced error signal

By substituting Eq. (4) into Eq. (1) and after some straightforward derivations, the M-TIADC output $Y(e^{j\omega})$ is expressed as

© IEICE 2016
DOI: 10.1587/elex.13.20160668
Received July 5, 2016
Accepted July 25, 2016
Publicized August 8, 2016
Copyedited August 25, 2016

IEICE Electronics Express, Vol.13, No.16, 1–12

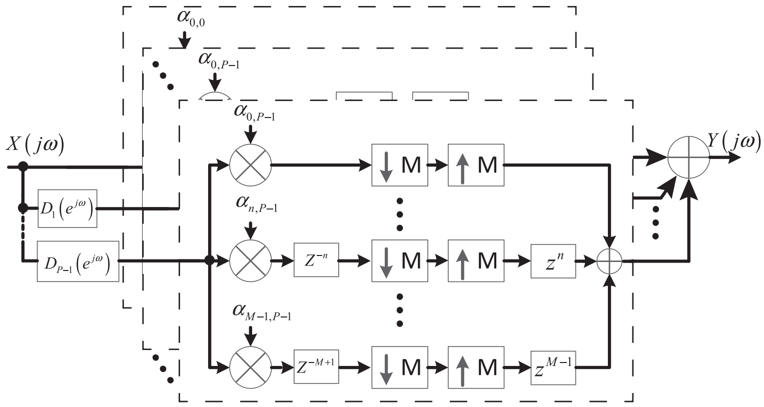

Fig. 2. A model for M-TIADC exploiting polynomial representation of channel frequency responses.

$$Y(e^{j\omega}) = \sum_{p=0}^{P-1} Y_p(j\omega) = \frac{1}{M}\sum_{p=0}^{P-1} \vec{X}_p^T \boldsymbol{E}\vec{\alpha}_p, \tag{5}$$

where

$$\vec{X}_p = \left[X^{(p)}(j\omega)\ X^{(p)}\left(j\left(\omega - \frac{2\pi}{M}\right)\right)\ \ldots\ X^{(p)}\left(j\left(\omega - \frac{2(M-1)\pi}{M}\right)\right)\right]^T, \tag{6}$$

$$\boldsymbol{E} = \begin{bmatrix} 1 & 1 & \cdots & 1 \\ 1 & e^{-j\frac{2\pi}{M}} & \cdots & e^{-j\frac{2(M-1)\pi}{M}} \\ \vdots & \vdots & \ddots & \vdots \\ 1 & e^{-j\frac{2(M-1)\pi}{M}} & \cdots & e^{-j\frac{2(M-1)(M-1)\pi}{M}} \end{bmatrix}, \tag{7}$$

$$\vec{\alpha}_p = [\alpha_{0,p}\quad \alpha_{1,p}\quad \ldots\quad \alpha_{M-1,p}]^T, \tag{8}$$

and

$$X^{(p)}(j\omega) = (j\omega)^p X(j\omega). \tag{9}$$

Exploiting the Hadamard matrix $\boldsymbol{F}$ of order M, which only consists of 1 and -1, and noting the facts that $\boldsymbol{F}\boldsymbol{F}^T = M\boldsymbol{I}$ ($\boldsymbol{I}$ is the identity matrix) and $\boldsymbol{F} = \boldsymbol{F}^T$, $Y_p(j\omega)$ is written as

$$Y_p(e^{j\omega}) = \vec{X}_p^T \boldsymbol{U}\vec{c}_p, \tag{10}$$

where

$$\vec{c}_p = \frac{1}{M}\boldsymbol{F}\vec{\alpha}_p \tag{11}$$

is the real-valued mismatch related coefficients and

$$\boldsymbol{U} = \frac{1}{M}\boldsymbol{E}\boldsymbol{F} \tag{12}$$

is the discrete Fourier transform (DFT) of real-valued Hadamard matrix $\boldsymbol{F}$. The following section reveals that the elements of $\vec{X}_p^T\boldsymbol{U}$ is the differential and modulated version of $X(j\omega)$.

2.3 Model of *M*-TIADC

By finding the inverse discrete-time Fourier transform (IDTFT) of Eq. (10), the p-th order output $Y_p(j\omega)$ in time-domain is

© IEICE 2016
DOI: 10.1587/elex.13.20160668
Received July 5, 2016
Accepted July 25, 2016
Publicized August 8, 2016
Copyedited August 25, 2016

IEICE Electronics Express, Vol.13, No.16, 1–12

$$y_p[n] = \sum_{k=0}^{M-1} c_{k,p} x^{(p)}[n] T_k[n], \tag{13}$$

where $T_k[n]$ is the repetition of the k-th row (column) vector of the Hadamard matrix $\boldsymbol{F}$, $x^{(p)}[n]$ is the IDTFT of $X^{(p)}(j\omega)$ and $c_{k,p}$ is the k-th element of $\vec{c}_p$. Thus the output $y[n]$ is written as

$$y[n] = \bar{x}[n] + \sum_{p=0}^{P-1} e_p[n], \tag{14}$$

where

$$\bar{x}[n] = \sum_{p=0}^{P-1} c_{0,p} x^{(p)}[n] \tag{15}$$

is the linearly distorted version of $x[n]$ and

$$e_p[n] = x^{(p)}[n] \sum_{k=1}^{M-1} c_{k,p} T_k[n] \tag{16}$$

is the p-th order mismatch induced error signal. Fig. 3 shows the model of M-TIADC corresponding to the mathematical expressions for output $y[n]$ presented in Eq. (14)–Eq. (16).

3 Calibration method

In this section, we propose our calibration method for FRMs in M-TIADC. In our approach, the error signal is reconstructed by the proposed differentiator-modulator structure utilizing the estimated mismatch coefficients.

3.1 Calibration structure

From the model presented in previous section, we conclude that the mismatch induced error signal can be generated using the derivative of input signal $x^{(p)}[n]$, the modulation sequences $T_k[n]$ and the mismatch coefficients $c_{k,p}$. However, only the M-TIADC output $y[n]$ is available. Under such circumstance, the mismatch induced error is reconstructed from $y[n]$ instead of $x[n]$. This replacement is reasonable because $y[n]$ is a good approximation of $x[n]$ in a well-designed TIADC. Thus the reconstructed error signal is

$$\hat{e}[n] = \sum_{p=0}^{P-1} \hat{e}_p[n] = \sum_{p=0}^{P-1} \sum_{k=1}^{M-1} \hat{c}_{k,p} y^{(p)}[n] T_k[n], \tag{17}$$

where $\hat{c}_{k,p}$ is the estimated mismatch coefficient for $c_{k,p}$ and $y^{(p)}[n]$ is the p-th order derivative of $y[n]$. Thus the calibrated TIADC output is

$$y^c[n] = y[n] - \hat{e}[n] = \bar{x}[n] + e[n] - \hat{e}[n]. \tag{18}$$

With ideal mismatch coefficients estimation, i.e. $\hat{c}_{k,p} = c_{k,p}$, the residual error signal is

$$\epsilon[n] = e[n] - \hat{e}[n] = \sum_{p=0}^{P-1} \sum_{k=1}^{M-1} (x^{(p)}[n] - y^{(p)}[n]) c_{k,p} T_k[n]. \tag{19}$$

© IEICE 2016
DOI: 10.1587/elex.13.20160668
Received July 5, 2016
Accepted July 25, 2016
Publicized August 8, 2016
Copyedited August 25, 2016

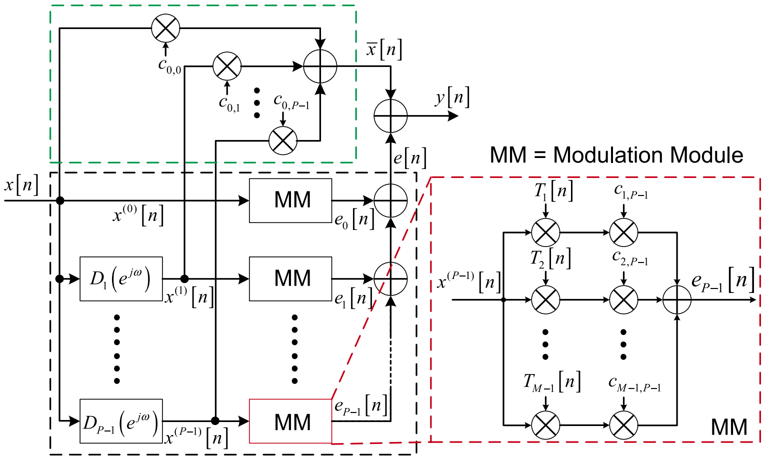

Fig. 3. Model of frequency responses mismatched M-TIADC.

As we ignore the linear distortion of the input signal, i.e. $\bar{x}[n] = x[n]$, the residual error signal is

$$\epsilon[n] = \sum_{p=0}^{P-1} \sum_{k=1}^{M-1} e^{(p)}[n] c_{k,p} T_k[n], \tag{20}$$

where $e^{(p)}[n]$ is the p-th order derivative of mismatch induced error signal $e[n]$. The proposed differentiator-modulator calibration structure for FRMs in M-TIADC is shown in Fig. 4. The differentiators $D_p(e^{(j\omega)})$ are implemented as real FIR filters and the modulation sequences $T_k[n]$ only consist of 1 and -1. The real-valued mismatch related coefficients $\hat{c}_{k,p}$ are estimated by the LS algorithm which is presented in the next section.

3.2 Estimation of mismatch coefficients

The calibration structure shown in Fig. 4 exploits the estimated mismatch coefficients $\hat{c}_{k,p}$ to reconstruct the mismatch induced error signal $\hat{e}[n]$. In this section, we introduce a foreground method to obtain the parameters $\vec{c}_p$.

A short training signal is required to estimate the mismatch parameters in our method. This requirement is easy to fulfill as training signal is a part of usual communication signals. There are few restrictions on the training signal. One

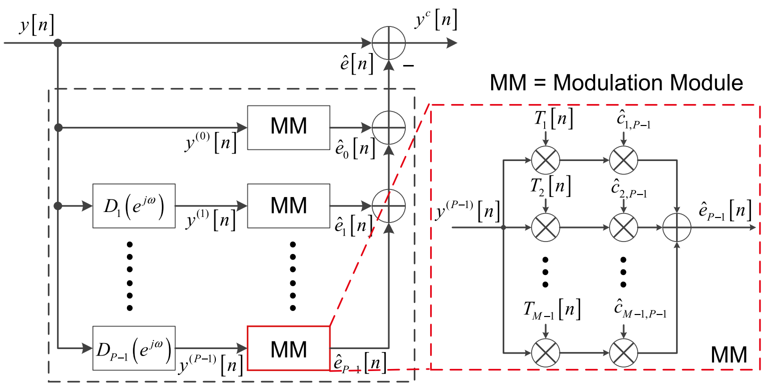

Fig. 4. Proposed differentiator-modulator calibration structure for FRMs in M-TIADC.

© IEICE 2016
DOI: 10.1587/elex.13.20160668
Received July 5, 2016
Accepted July 25, 2016
Publicized August 8, 2016
Copyedited August 25, 2016

restriction is that it should be wide-band signal because the FRMs are frequency dependent. Another restriction is that it should longer than MP samples otherwise the LS problem is under determined.

Denoting

$$\vec{y}[n] = [y[n] \quad y[n-1] \quad \cdots \quad y[0]]^T, \tag{21}$$

$$\vec{x}_{p,k}[n] = [x^{(p)}[n]T_k[n] \quad x^{(p)}[n-1]T_k[n-1] \quad \cdots \quad x^{(p)}[0]T_k[0]]^T, \tag{22}$$

and

$$\boldsymbol{X}_p = [\vec{x}_{p,0}\ \vec{x}_{p,1}\ \cdots\ \vec{x}_{p,M-1}], \tag{23}$$

then the time-domain TIADC output Eq. (14) is rewritten in matrix form

$$\vec{y}[n] = \boldsymbol{X}\vec{c} \tag{24}$$

with

$$\boldsymbol{X} = [\boldsymbol{X}_0\ \boldsymbol{X}_1\ \cdots\ \boldsymbol{X}_{P-1}] \tag{25}$$

and

$$\vec{c} = [\vec{c}_0\ \vec{c}_1\ \cdots\ \vec{c}_{P-1}]. \tag{26}$$

Thus $\vec{c}$ can be estimated by the LS method utilizing the following equation

$$\hat{\vec{c}} = (\boldsymbol{X}^T\boldsymbol{X})^{-1}(\boldsymbol{X}^T\vec{y}[n]). \tag{27}$$

It should be noted that the size of matrix $\boldsymbol{X}^T\boldsymbol{X}$ is $MP \times MP$. Thus the computation of matrix inversion won't cost many resources as M and P are relatively small in practice.

3.3 Cascade calibration structure

In order to further suppress the error signal and improve the performance, a cascade calibration structure is presented as shown in Fig. 5.

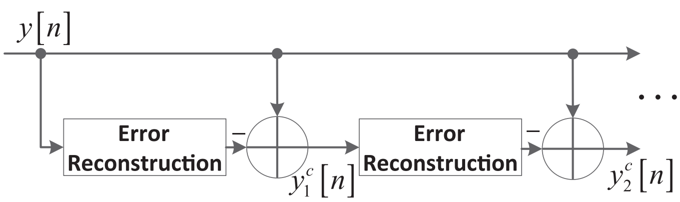

Fig. 5. Cascade calibration structure.

Denoting the i stage compensation output and residual error as $y_i^c[n]$ and $\epsilon_i[n]$ respectively, then the $i+1$ stage residual error is

$$\epsilon_{i+1}[n] = \sum_{p=0}^{P-1}\sum_{k=1}^{M-1}(x^{(p)}[n] - y_i^{c(p)}[n])c_{k,p}T_k[n], \tag{28}$$

where $y_i^{c(p)}[n]$ is the p-th order derivative of $y_i^c[n]$. As we ignore the linear distortion of $x[n]$, $\epsilon_{i+1}[n]$ is rewritten as

$$\epsilon_{i+1}[n] = \sum_{p=0}^{P-1}\sum_{k=1}^{M-1}\epsilon_i^{(p)}[n]c_{k,p}T_k[n], \tag{29}$$

© IEICE 2016
DOI: 10.1587/elex.13.20160668
Received July 5, 2016
Accepted July 25, 2016
Publicized August 8, 2016
Copyedited August 25, 2016

where $\epsilon_i^{(p)}[n]$ is the p-th order derivative of $\epsilon_i[n]$. The energy of $\epsilon_{i+1}[n]$ is much lower than the energy of $\epsilon_i[n]$ because the mismatch coefficients $c_{k,p} \ll 1$ ($k = 1, 2, \cdots, M-1$; $p = 0, 1, \cdots, P-1$) and the elements of modulation sequence $T_k[n]$ are either 1 or -1.

The ultimate compensation performance of our method is the same as the method presented in [8]. The calibration performances of both methods are bounded by modeling accuracy, the filter approximation errors, the nonlinearity of individual ADCs and the system noise such as quantization noise.

4 Simulation results

In this section, numerical simulation results are presented to demonstrate the performance of the proposed calibration method. The channel frequency responses are first-order low-pass filters with individual cutoff frequencies, gains and timing offsets. The parameters for frequency responses in simulated 4-TIADC and 8-TIADC are shown in Table I. The resolution of the simulated TIADCs is 12 bits.

Table I. Parameters for frequency responses. F_n^c, g_n and Δ_n are the cutoff frequency, gain and timing offset of channel n respectively.

4-TIADC				8-TIADC			
n	$F_n^c(F_s)$	g_n	$\Delta_n(T_s)$	n	$F_n^c(F_s)$	g_n	$\Delta_n(T_s)$
0	4	1.01	−0.004	0	4.11	1.02	−0.01
1	3.94	0.99	−0.003	1	4.02	1.01	0.008
2	3.97	1	0.002	2	3.88	0.99	0.01
3	4.05	1.01	0.004	3	3.99	1	−0.01
				4	4.1	0.98	0.009
				5	4.01	1.02	−0.008
				6	3.95	1	−0.007
				7	3.90	0.97	−0.009

Fig. 6 shows the spectra of a 4-TIADC output signal before and after calibration. The input is a wide-band signal with 11 tones spanning from 0 to $0.5F_s$. Figures (a), (b) and (c) in Fig. 6 are the spectra before calibration, after one-stage calibration and after two-stage calibration respectively. The signal-to-noise ratio (SNR) of the uncalibrated signal is 41.4 dB, while the SNR of calibrated signals are 59.3 dB for one-stage compensation and 62.7 dB for two-stage compensation. The mismatch induced spurs are suppressed greatly as the figures show. The spurious-free dynamic ranges (SFDRs) are 38 dB, 56.7 dB and 73.9 dB for figure (a), (b) and (c) respectively. The mismatch coefficients are estimated using a wide-band training signal with 8 tones spanning from 0 to $0.5Fs$.

The spectra of 8-TIADC output signal before and after compensation are shown in Fig. 7. The input signal and the training signal are the same as in Fig. 6. The SNR of uncalibrated 8-TIADC output is 33.8 dB, while the SNRs of one-stage and two-stage calibrated signal are 52.9 dB and 60.8 dB respectively. The SFDRs are 36.6 dB, 54.3 dB and 63.9 dB for figure (a), (b) and (c) respectively. The calibration performance in 8-TIADC is not as good as in 4-TIADC. This is because there are

© IEICE 2016
DOI: 10.1587/elex.13.20160668
Received July 5, 2016
Accepted July 25, 2016
Publicized August 8, 2016
Copyedited August 25, 2016

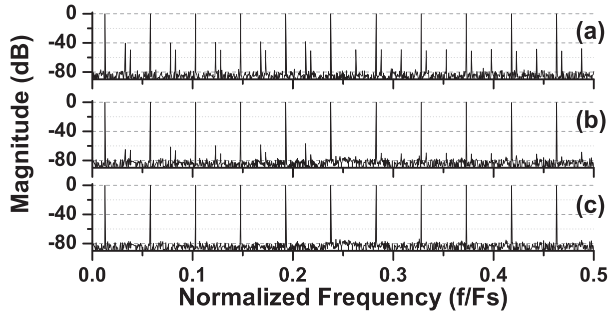

Fig. 6. Spectra of frequency response mismatched 4-TIADC output. (a) before calibration, (b) after one-stage calibration and (c) after two-stage calibration.

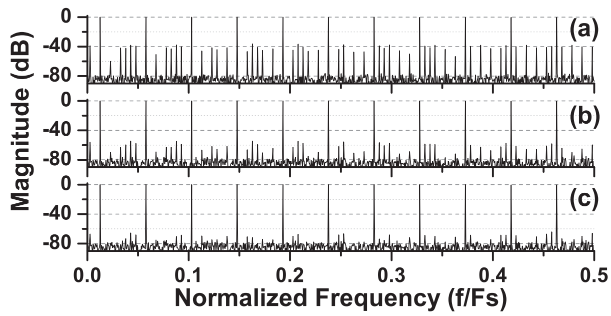

Fig. 7. Spectra of frequency response mismatched 8-TIADC output. (a) before calibration, (b) after one-stage calibration and (c) after two-stage calibration.

more parameters to estimate in 8-TIADC, and with the same training signal the estimation precision degrades as number of parameters increases.

Figures in Fig. 8 show the SNR improvement versus the length of training signal in 4-TIADC (a) and in 8-TIADC (b). The training signal is a wide-band signal with 8 tones as in previous simulations. The calibration performance increases with the length of training signal in both 4-TIADC and 8-TIADC. Longer training signal is required to gain the same SNR improvement for 8-TIADC compared with 4-TIADC as there are more mismatch parameters to estimate. It should be noted that the SNR improvements with different order of polynomial series are almost the same for both 4-TIADC and 8-TIADC. Thus a 3rd-order polynomial series is sufficient to model the first-order low-pass filters used as frequency responses in this paper. From the figures in Fig. 8 we can conclude that a training signal with 2^{11} to 2^{12} samples is enough estimate the mismatch parameters accurately.

Fig. 9 illustrates the SNR improvement versus the order of differentiators and the length of training signal for 4-TIADC (a) and 8-TIADC (b). For a fixed order of differentiator, the SNR improvement increases with the length of training signal, which is demonstrated by Fig. 8. The calibration performance also increases with the differentiator order for all simulated training signal lengths. However, the SNR improvement only increases by a small number with the order of differentiator for short training signal. We can conclude that differentiators with about 10 and 20 taps are sufficient for calibration with short and long training signal respectively.

© IEICE 2016
DOI: 10.1587/elex.13.20160668
Received July 5, 2016
Accepted July 25, 2016
Publicized August 8, 2016
Copyedited August 25, 2016

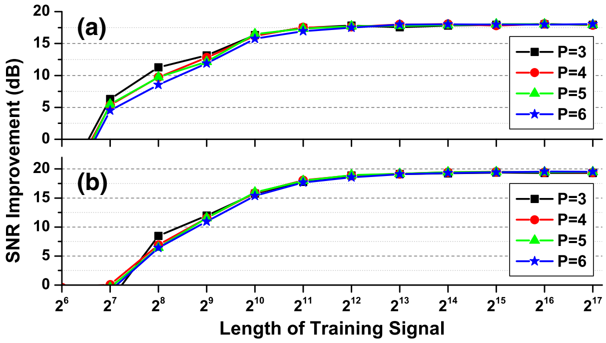

Fig. 8. SNR improvement versus length of training signal under different order of polynomial series. (a) 4-TIADC; (b) 8-TIADC.

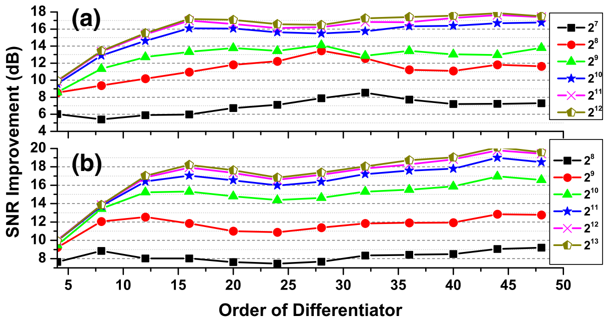

Fig. 9. SNR improvement versus order of differentiator under different length of training signal. (a) 4-TIADC; (b) 8-TIADC.

A brief comparison between several state-of-the-art FRM calibration methods is shown in Table II. Compared with the blind calibration methods [10, 13], the method in this work has wider applications as the blind methods only focus either on 4-TIADC or 2-TIADC while our method is for M-TIADC where $M = 2, 4, 8, \cdots$. While compared with the time-varying filters based methods [8, 9], our method is much simpler in terms of implementation because only time-invariant signal processing is required thus coefficients updating for variable digital

Table II. A brief comparison between calibration methods for FRMs in TIADCs.

Reference	[8]	[9]	[10]	[13]	This work
Estimation Strategy	None	Missing samples	Over-sampling	Circularity	Training signal
Channel No.	M	M	2	4	M
Samples	\	2×10^3	10^6	3×10^3	2.62×10^5
Complexity	1 real VDF	1 real VDF	2P-1 real FIR	3 complex FIR	P-1 real FIR
Bandwidth	π	π	π	0.8π	0.8π

© IEICE 2016
DOI: 10.1587/elex.13.20160668
Received July 5, 2016
Accepted July 25, 2016
Publicized August 8, 2016
Copyedited August 25, 2016

ELectronics EXpress

lter (VDF) at every samples is avoided. Moreover, on-line calibration is possible when training sequences are contained in the input signal, which is the case of many communication signals such as OFDM.

5 Conclusion

A digital compensation method for FRMs in M-TIADCs is presented in this brief. In this method, the frequency responses are represented by polynomial series in $j\omega$, and the error signal is reconstructed by fixed differentiator FIR filters and modulation sequences which only consist of 1 and -1. Compared with conventional methods, our method is more efficient and simpler as no extra front-end hardware, time-varying filter or complex signal processing unit is required.

© IEICE 2016
DOI: 10.1587/elex.13.20160668
Received July 5, 2016
Accepted July 25, 2016
Publicized August 8, 2016
Copyedited August 25, 2016